

# Interfacial Microstructure and Bonding Strength of Copper Cladding Aluminum Rods Fabricated by Horizontal Core-Filling Continuous Casting

YA-JUN SU, XIN-HUA LIU, HAI-YOU HUANG, XUE-FENG LIU, and JIAN-XIN XIE

Copper cladding aluminum (CCA) rods with a diameter of 30 mm and a sheath thickness of 3 mm were fabricated by horizontal core-filling continuous casting (HCFC) technology. The microstructure and morphology, distribution of chemical components, and phase composition of the interface between Cu and Al were characterized by scanning electron microscope (SEM), transmission electron microscope (TEM), and energy dispersive spectrometer (EDS). The formation mechanism of the interface and the effects of key processing parameters, *e.g.*, aluminum casting temperature, secondary cooling intensity, and mean withdrawing speed on the interfacial microstructure and bonding strength were investigated. The results show that the CCA rod has a multilayered interface, which is composed of three sublayers—sublayer I is  $\text{Cu}_9\text{Al}_4$  layer, sublayer II is  $\text{CuAl}_2$  layer, and sublayer III is composed of  $\alpha\text{-Al}/\text{CuAl}_2$  pseudo eutectic. The thickness of sublayer III, which occupies 92 to 99 pct of the total thickness of the interface, is much larger than the thicknesses of sublayers I and II. However, the interfacial bonding strength is dominated by the thicknesses of sublayers I and II; *i.e.*, the bonding strength decreases with the rise of the thicknesses of sublayers I and II. When raising the aluminum casting temperature, the total thickness of the interface increases while the thicknesses of sublayers I and II decrease and the bonding strength increases. Either augmenting the secondary cooling intensity or increasing the mean withdrawing speed results in the decrease in both total thickness of the interface and the thicknesses of sublayers I and II, and an increase in the interfacial bonding strength. The CCA rod with the largest interfacial bonding strength of  $67.9 \pm 0.5$  MPa was fabricated under such processing parameters as copper casting temperature 1503 K (1230 °C), aluminum casting temperature 1063 K (790 °C), primary cooling water flux 600 L/h, secondary cooling water flux 700 L/h, and mean withdrawing speed 87 mm/min. The total thickness of the interface of the CCA rod fabricated under the preceding processing parameters is about 75  $\mu\text{m}$ , while the thicknesses of sublayers I and II are about 1.1 and 0.1  $\mu\text{m}$ , respectively.

DOI: 10.1007/s11661-011-0785-x

© The Minerals, Metals & Materials Society and ASM International 2011

## I. INTRODUCTION

SINCE the 1960s, copper cladding aluminum (CCA) bimetallic composite has been widely used in the fields of signal transportation, power transmission, special electromagnetic wire, *etc.* because of its outstanding comprehensive performances, for example, high conductivity, excellent corrosion resistance, low density, good brazing property, and high cost-performance ratio.<sup>[1–4]</sup>

With the application of CCA in industry, more and more scientists and engineers have taken an interest in the development of fabricating technologies of CCA products. So far, there are several methods for fabricating CCA composites, but only the co-rolling<sup>[5]</sup>

method and overlay welding<sup>[6]</sup> method have already been applied in manufacturing CCA wire for industrial production. Both methods belong to the category of solid-solid bonding technology and have some shortcomings, such as long process flow, high production costs, serious environmental issues during surface treatment, and difficulty in preparing composite conductors with heteromorphic or large cross section, *e.g.*, flat bus used for large electric current transmission. Therefore, Neumann<sup>[7]</sup> and Xie *et al.*<sup>[8,9]</sup> individually invented a vertical core-filling continuous casting (VCFC) technology to fabricate the metal cladding materials. Then, Xie and co-workers<sup>[10,11]</sup> developed a novel method of horizontal core-filling continuous casting (HCFC) technology based on VCFC technology. HCFC technology is not only convenient for obtaining an impurity-free interface but is also suitable for industrialization. When preparing bimetallic composites by VCFC or HCFC technology, the dissimilar liquid metals were cast and bonded simultaneously. The bonding process was realized when liquid core metal filled into the presolidified metal sheath and solidified. Therefore, VCFC and

YA-JUN SU, XIN-HUA LIU, HAI-YOU HUANG, XUE-FENG LIU, and JIAN-XIN XIE are with the Key Laboratory for Advanced Materials Processing (MOE), University of Science and Technology Beijing, Beijing 100083, P.R. China. Contact e-mail: jxxie@mater.ustb.edu.cn

Manuscript submitted November 16, 2010.

Article published online August 10, 2011

HCFC technologies can be classified into the category of liquid-solid bonding technology.

As is well known, the physical and mechanical properties of Al/Cu bimetallic composite are influenced remarkably by the thickness and microstructure of the interface.<sup>[12–14]</sup> The authors' previous research found<sup>[11]</sup> that there was no regular variation of interfacial bonding strength with the total thickness of the interface of CCA rods prepared by HCFC. It can be seen from the Cu-Al binary alloy phase diagram<sup>[15]</sup> that chemical reactions between copper and aluminum could occur easily to generate several intermetallic compounds. Therefore, the phase composition and microstructure of the interface might be the major factors that affect the interfacial bonding strength of CCA.<sup>[13,16]</sup> In this work, the microstructure and morphology, chemical components distribution, phase composition, and bonding strength of the interface of CCA rods prepared by HCFC were investigated. Subsequently, based on the previous research results of the feasible processing window for preparing CCA rods by HCFC, the effects of key processing parameters, such as aluminum casting temperature, secondary cooling water flux, and mean withdrawing speed on the microstructure and bonding strength of the interface, were analyzed, respectively. Finally, the optimal processing parameters within the scope of this study were determined according to a criterion of the largest interfacial bonding strength.

## II. EXPERIMENTAL PROCEDURES

### A. Fabrication Process of CCA Rods

Figure 1 showed the schematic diagram of the HCFC device (Figure 1(a)) and the detailed structure of the composite mold (Figure 1(b)). The fabricating process of CCA rods could be described briefly as follows: First, liquid copper in crucible 2 was insufflated into composite mold 5 continuously *via* the heating cylinder in the composite mold holding furnace 4 and solidified into a copper tube. Then, liquid aluminum in crucible 1 was injected into the presolidified copper tube continuously

through mandrel 10 and solidified into aluminum core, which metallurgically combined with the copper sheath. Finally, CCA rod was continuously pulled out of the composite mold and by the secondary cooling zone 6. A more detailed description of the preparation process can be seen in the literature.<sup>[11]</sup>

The previous research<sup>[11]</sup> showed that CCA rods were prepared with an HCFC device illustrated in Figure 1 in reasonable processing parameters ranges (feasible processing windows) as follows: copper casting temperature  $T_{Cu} = 1503$  K (1230 °C), aluminum casting temperature  $T_{Al} = 1043$  K to 1123 K (770 °C to 850 °C), primary cooling water flux  $Q_1 = 600$  L/h, secondary cooling water flux  $Q_2 = 600$  to 800 L/h, and mean withdrawing speed  $v = 60$  to 87 mm/min in an intermittent withdrawal mode. CCA rods had high surface quality and uniform sheath thickness without macrocasting defect and interface defect. Based on the preceding results, CCA rods with a diameter of 30 mm and a sheath thickness of 3 mm were fabricated under the processing conditions as shown in Table I using 99.9 wt pct pure copper (C11000) and 99.7 wt pct pure aluminum (1070) in this work. All CCA rods prepared in our experiments were more than 10-m long. Figure 2 shows the macromorphology of a CCA rod fabricated by HCFC. The surface roughness of the as-cast CCA

**Table I. Processing Parameters of Fabricating CCA Rods by HCFC**

Number	$T_{Al}$ [K (°C)]	$Q_2$ (L/h)	$v$ (mm/min)
1	1043 (770)	600	60
2	1063 (790)	600	60
3	1083 (810)	600	60
4	1123 (850)	600	60
5	1063 (790)	600	67
6	1063 (790)	700	67
7	1063 (790)	800	67
8	1063 (790)	700	75
9	1063 (790)	700	87

Note:  $T_{Al} = 1503$  K (1230 °C), and  $Q_2 = 600$  L/h.

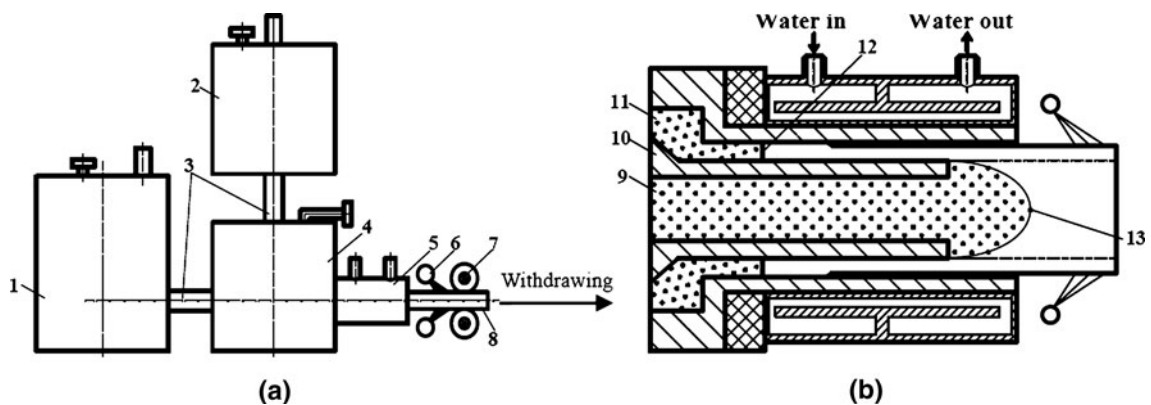


Fig. 1—Schematic diagram of the HCFC device for preparing CCA rod: (a) device and (b) composite mold: 1—molten aluminum holding furnace, 2—molten copper holding furnace, 3—runner, 4—composite mold holding furnace, 5—composite mold, 6—secondary cooling, 7—pinch rolls, 8—CCA rod, 9—liquid aluminum, 10—mandrel, 11—liquid copper, 12—solidification front of liquid copper, and 13—solidification front of liquid aluminum.

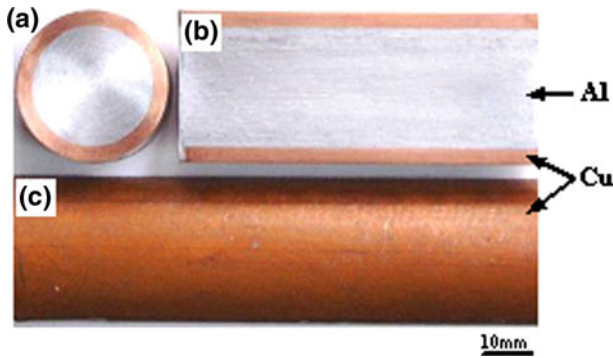


Fig. 2—Macromorphologies of the CCA rod: (a) cross section, (b) longitudinal section, and (c) surface ( $T_{\text{Cu}} = 1503 \text{ K}$  (1230 °C),  $T_{\text{Al}} = 1043 \text{ K}$  (770 °C),  $v = 60 \text{ mm/min}$ , and  $Q_1 = Q_2 = 600 \text{ L/h}$ ).

rod was measured with a Dektak150 surface profiler (Veeco Instruments Inc., Plainview, NY). The results show that the surface roughness of the rod was  $Ra = 87 \pm 3 \text{ nm}$ , which reached that of a machined work piece.

### B. Testing and Analysis Methods

Cross-section samples with 10-mm thickness were cut from CCA rods by an electrical spark linear cutting machine (ESLCM) for interfacial morphology observation and interfacial shear strength test. The interface morphologies of the samples were observed after mechanical polishing and etched by a reagent of HF(1 mL):HNO<sub>3</sub>(2.5 mL):H<sub>2</sub>O(95 mL). The samples for transmission electron microscope (TEM) were prepared as follows: a cross-section disc with a thickness of 0.5 mm was cut from the CCA rod with ESLCM. A TEM specimen with a diameter of 3 mm was taken from the disc carefully, and the TEM specimen must include the complete interface. Then, the thickness of the TEM specimen was reduced to about 30  $\mu\text{m}$  with diamond sandpaper and to about 100 nm with argon ion milling.

The interfacial morphologies were observed with a XJZ-6A optical microscope and a Leica S440i scanning electron microscope (SEM) (Leica Microsystems Ltd., Wetzlar, Germany). The thicknesses of the interface and its sublayers were measured with the SEM. The distributions of Al and Cu in the interface and its sublayers were analyzed with an Oxford-7060 X-ray energy dispersive spectrometer (EDS) (Oxford Instruments, Oxfordshire, UK). The micromorphology of each phase in the interface was observed with a TF20 field-emission TEM. The microstructures of all phases were also characterized by selective area electron diffraction (SAED). The microhardness of each sublayer was measured using a nanoindenter (MTS Nano Indenter, MTS Systems Corporation, Eden Prairie, MN) with a given indent depth of 200 nm.

The interfacial bonding strength of CCA rods was tested with a shear strength tester, as shown in Figure 3, which was mounted in a 20-ton universal testing machine. A continuous load was applied on the sample with a thickness of 10 mm *via* a punch 1 until the

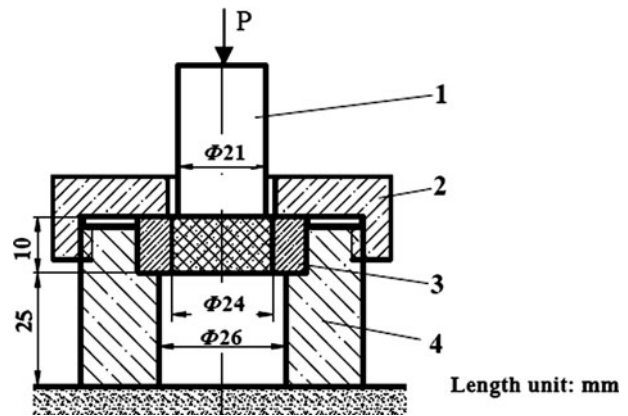


Fig. 3—Schematic diagram of the shear strength tester: 1—punch, 2—gland bush, 3—CCA rod sample, and 4—die (gland bush 2 connects with die 4 by screwed connection).

interface of the sample was failed. The maximum load  $P_{\text{max}}$  was recorded and the diameter of the shear cylinder of the deformed sample ( $d$ ) was measured with a vernier caliper. The interfacial shear strength ( $\tau$ ) was calculated according to the following equation:

$$\tau = \frac{P_{\text{max}}}{A} = \frac{P_{\text{max}}}{\pi dh} \quad [1]$$

where  $A$  is the area of shear plane and  $h = 10 \text{ mm}$  is the thickness of samples.

## III. EXPERIMENTAL RESULTS

### A. Microstructure of the Interface

Figure 4 illustrates the interfacial micromorphology of the CCA rod prepared under the processing conditions  $T_{\text{Cu}} = 1503 \text{ K}$  (1230 °C),  $T_{\text{Al}} = 1043 \text{ K}$  (770 °C),  $Q_1 = Q_2 = 600 \text{ L/h}$ , and  $v = 60 \text{ mm/min}$  (processing parameter 1 in Table I). It can be seen from Figure 4 that there is a 160- $\mu\text{m}$ -thick interface between the copper sheath and aluminum core, and the boundaries on both sides of the interface are smooth (Figures 4(a), (b), and (d)). Along the radial orientation from the copper sheath to the aluminum core, the interface can be divided into three sublayers with different thicknesses and morphologies (Figures 4(b) through (d)). Sublayer I with a thickness of about 1.7  $\mu\text{m}$  is the narrowest with a basically straight boundary with sublayer II. Sublayer II with its thickness of about 2.8  $\mu\text{m}$  has a cellular boundary with sublayer III. Sublayer III with its thickness of approximately 155.5  $\mu\text{m}$  has a distinct feature of cellular-like eutectic morphology. The total thickness of sublayers I and II occupied only 2.8 pct of the thickness of the interface.

### B. Chemical Components Distribution of the Interface

The contents of copper and aluminum at measure points 1 through 16 marked in Figures 4(b) through (d) were measured by EDS point analysis. The results were

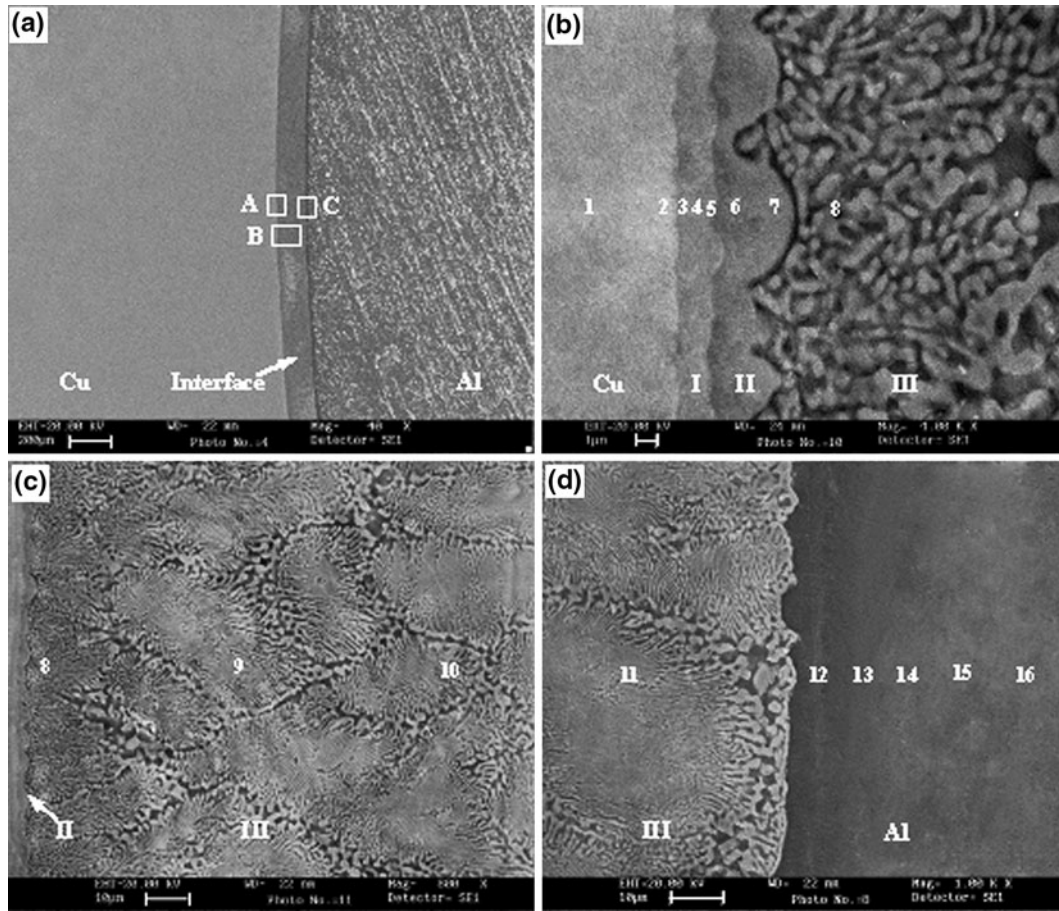


Fig. 4—SEM micrographs of the interface of CCA rod (refer to Fig. 2(a)). (a) Micromorphology near the interface on the cross section; and (b), (c), and (d) the partial enlarged details of sections A, B, and C in (a), respectively. I—sublayer I, II—sublayer II, and III—sublayer III.

**Table II. Concentration of Cu and Al on Each Point in or near the Interface (Reference to Fig. 4)**

Measure Point		Chemical Composition		Measure Point		Chemical Composition	
Location	No.	$\omega_{\text{Cu}}$ (At. Pct)	$\omega_{\text{Al}}$ (At. Pct)	Location	No.	$\omega_{\text{Cu}}$ (At. Pct)	$\omega_{\text{Al}}$ (At. Pct)
Copper sheath	1	100.0	0	sublayer III	9	17.0	83.0
	2	99.9	0.1		10	17.2	82.8
Sublayer I	3	98.3	1.7	aluminum core	11	16.3	83.7
	4	89.1	10.9		12	0.3	99.7
	5	65.6	34.4		13	0.2	99.8
Sublayer II	6	32.6	67.4	14	0	100.0	
	7	32.6	67.4	15	0.2	99.8	
Sublayer III	8	14.9	85.1	16	0	100.0	

Note:  $\omega_{\text{Cu}}$  = the content of copper, and  $\omega_{\text{Al}}$  = the content of aluminum.

tabulated in Table II. Table II indicates that the content of aluminum showed an increasing tendency while that of copper illustrated a decreasing tendency along the radial orientation from copper sheath to aluminum core. Little aluminum was found in the matrix of the copper sheath adjacent to the interface (points 1 to 2). In sublayer I, the atomic percent of aluminum rose from 1.7 at. pct at point 3 to 34.4 at. pct at point 5, while that of copper fell from 98.3 at. pct at point 3 to 65.6 at. pct at point 5. In sublayer II,

the atomic percents of copper and aluminum at points 6 and 7 were the same as the aluminum-to-copper ratio of approximately 2:1. In sublayer III, the atomic percents of aluminum at four measure points (points 8 through 11) were around 83.7 at. pct (the average value of the four points), while those of copper were in the vicinity of 16.3 at. pct (average value) with Al/Cu of 4.8 to 5.7. Hardly any copper was found in the matrix of the aluminum core adjacent to the interface (points 12 through 16).

In order to clearly understand the continuous distributions of copper and aluminum in the interface of CCA rod, the contents of copper and aluminum were also detected by EDS line scanning analysis. Line scanning tracks were shown as lines AB, CD, and EF in Figures 5(a), (d), and (g), and the results are illustrated in Figures 5(b) and (c), Figures 5(e) and (f), and Figures 5(h) and (i), respectively. Table II and Figures 5(b) and (c) indicated that, except the interface, either aluminum content in copper sheath or copper content in aluminum core was few. This suggests that the reaction or diffusion between aluminum and copper occurred just in the range of the interface. Along the line scanning track of CD or EF (from copper sheath to aluminum core), aluminum content gradually increased in sublayer I and remained constant in sublayers II and III, while copper content decreased in sublayer I and remained constant in sublayers II and III (Figures 5(e) through (i)). In addition, there were remarkable leaps of aluminum or copper content between sublayers II and III (Figures 5(e) and (f)) and between sublayer III and the aluminum core (Figures 5(h) and (i)). According to Table II and Figure 5, the thickness of the alloyed range induced by the dissolution of Cu is the same as that of the final interface.

Furthermore, Table II and Figure 5 also show that the Al or Cu concentration gradient varies in different regions of the interface. It can be calculated based on the data in Table II that the Al or Cu concentration gradient in sublayer I is approximately  $19.2 \text{ at. pct } \mu\text{m}^{-1}$ , while those in sublayers II and III are about  $0 \text{ at. pct } \mu\text{m}^{-1}$ , respectively.

### C. Phase Composition of the Interface

According to the preceding analyses on the contents of copper and aluminum in the interface and Al-Cu binary alloy phase diagram,<sup>[15]</sup> the interface of CCA rod should consist of solid solution phase and intermetallic compound phase. Figures 6(a) through (c) showed TEM micrographs and SAED patterns of sublayers I, II, and III. Figures 6(d) through (h) illustrated the calibrations of the SAED patterns. Figure 6 suggests that sublayer I was composed of intermetallic compound  $\text{Cu}_9\text{Al}_4$  (Figures 6(a) and (e)); sublayer II consisted of intermetallic compound  $\text{CuAl}_2$  (Figures 6(b) and (f)); and sublayer III was a pseudo eutectic zone, which was made up of solid solution  $\alpha\text{-Al}$  and intermetallic compound  $\text{CuAl}_2$  (Figures 6(c), (g), and (h)). The content and distribution of  $\text{CuAl}_2$  phase in sublayer III was also calculated based

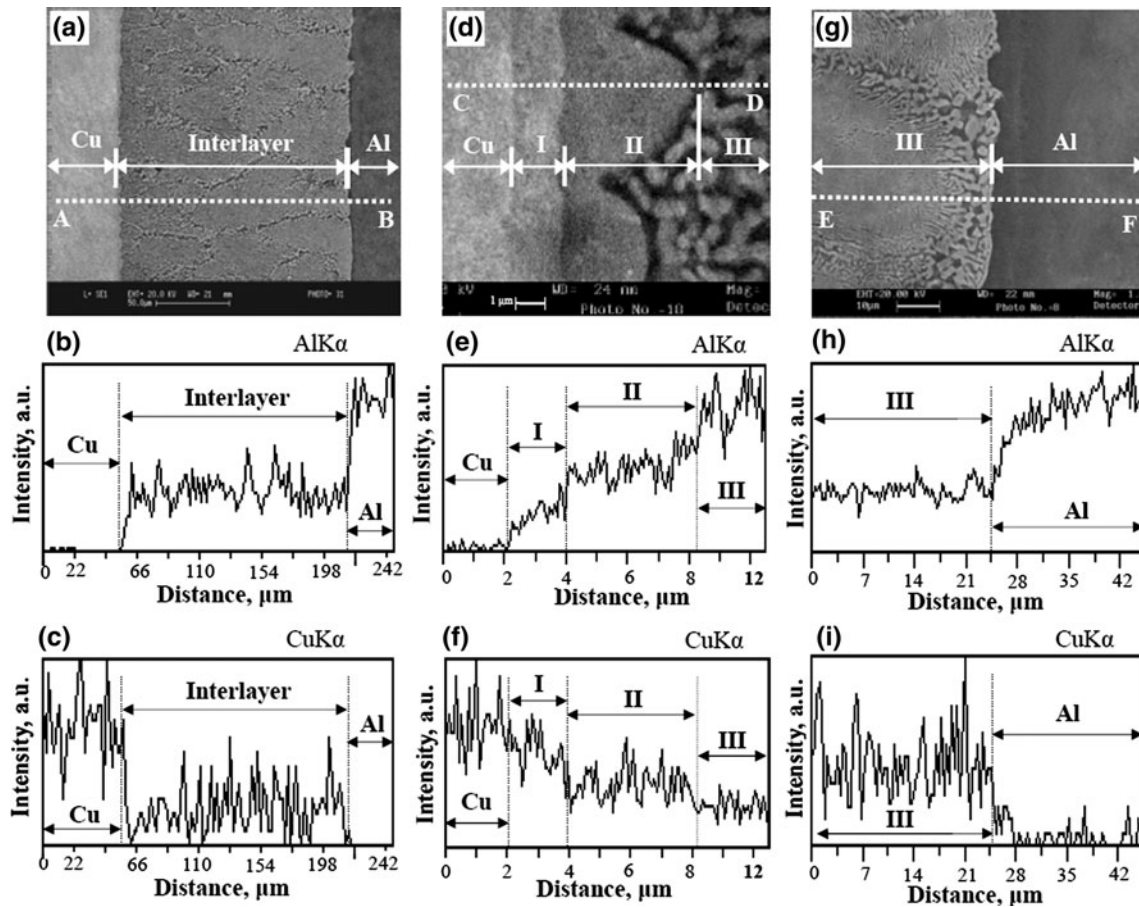


Fig. 5—EDS line scanning analysis on the chemical components' distribution in or near the interface (reference to Fig. 4). (a), (d), and (g) illustration of EDS line scanning tracks; and (b) and (c), (e) and (f), and (h) and (i) aluminum or copper content distribution diagrams along the line AB in (a), CD (d), and EF in (g), respectively. I—sublayer I, II—sublayer II, and III—sublayer III.

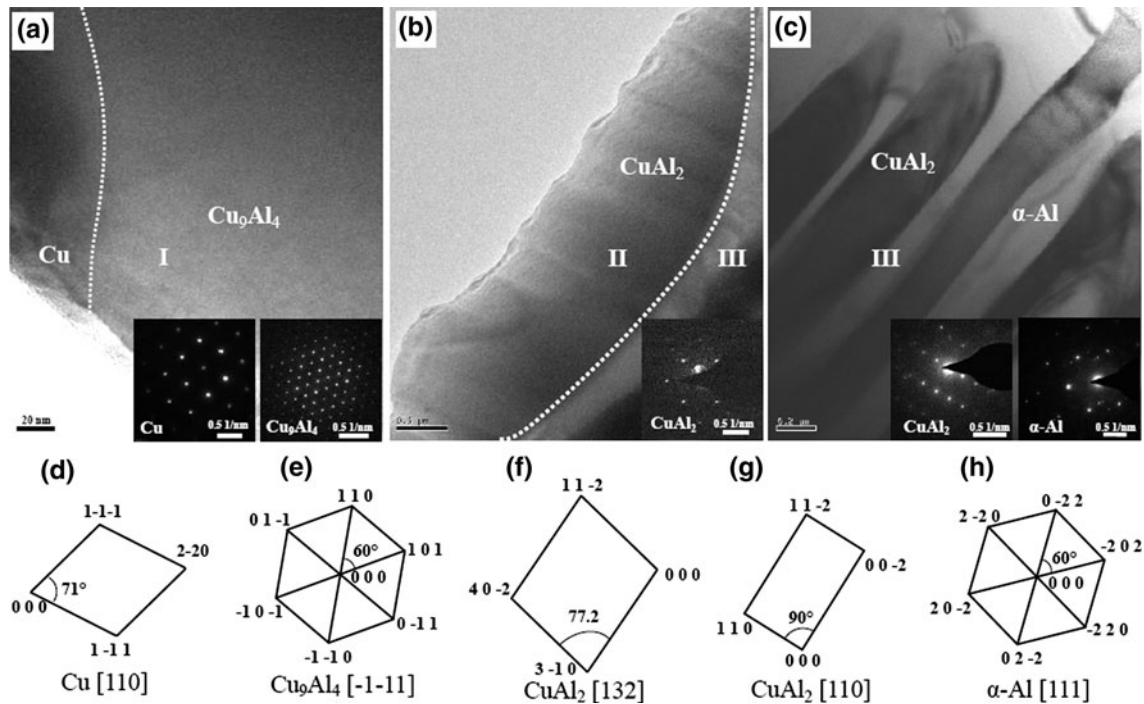


Fig. 6—TEM micrographs and SAED patterns with their calibrations of all phases in the interface (refer to Figs. 4 and 5). (a), (d), and (e) TEM micrographs, SAED patterns, and calibration of pure copper phase in copper sheath and  $\text{Cu}_9\text{Al}_4$  phase in sublayer I, respectively. (b) and (f) TEM micrograph and SAED pattern of  $\text{CuAl}_2$  phase in sublayer II. (c), (g), and (h) TEM micrographs of  $\alpha\text{-Al}/\text{CuAl}_2$  pseudo eutectic zone and SAED patterns of  $\text{CuAl}_2$  phase and  $\alpha\text{-Al}$  phase, respectively. I—sublayer I, II—sublayer II, and III—sublayer III.

on a  $28471.4 \mu\text{m}^2$  area of the interface in Figure 5(a). The results show that the content of the  $\text{CuAl}_2$  phase is a constant of about 44 pct in sublayer III.

In order to understand the mechanical properties of the intermetallic compounds in the interface, the hardness was measured and the results showed that the hardnesses of the  $\text{Cu}_9\text{Al}_4$  phases in sublayer I and the  $\text{CuAl}_2$  phases in sublayer II are 6.3 to 8.0 GPa and 4.5 to 5.7 GPa, respectively, and the hardness of the  $\alpha\text{-Al}/\text{CuAl}_2$  pseudo eutectic in sublayer III is 2.3 to 3.9 GPa.

#### D. Bonding Strength of the Interface

The interfacial bonding strength of the CCA rod fabricated on the processing condition of  $T_{\text{Cu}} = 1503 \text{ K}$  ( $1230 \text{ }^\circ\text{C}$ ),  $T_{\text{Al}} = 1043 \text{ K}$  ( $770 \text{ }^\circ\text{C}$ ),  $Q_1 = Q_2 = 600 \text{ L/h}$ , and  $v = 60 \text{ mm/min}$  (processing parameter 1 in Table I) was measured by shear testing and the interfacial shear strength ( $\tau$ ) was  $45.2 \pm 0.7 \text{ MPa}$ . Considering the tensile strength and the shear strength of pure aluminum (1070) used in our experiments are 60 to 100 MPa and 30 to 50 MPa<sup>[17]</sup> at room temperature, respectively, the interfacial bonding strength of the CCA rod reached the shear strength of aluminum core, which indicated that a firm metallurgical bonding between copper sheath and aluminum core could be attained by HCFC technology.

Figure 7 showed the micromorphology of the shear fractograph of the CCA rod after shear testing. The fractograph illustrated a distinct river pattern, which consisted of a group of shear lips (Figure 7(a)). The orientation and the shear-lip interval of the pattern in

different regions (areas A, B, and C) varied, as shown in Figures 7(b), (c), and (d), respectively. In order to determine the exact fracture location in the interface, the chemical component measurement of the eight points on the fracture surface marked 1 through 8 in Figure 7(a) was performed by the EDS point scanning analysis, and the results are tabulated in Table III. From Figures 4 and 7, and Tables II and III, it can be inferred that the shear failure occurs mainly in the region between sublayers I and III of the interface. That is, the shear failure occurs mainly in sublayer II. The reasons for it are as follows: (1) sublayer II is thicker than sublayer I, (2) the plastic deformability of sublayer II is worse than that of sublayer III, and (3) the shear failure has difficulty occurring in the aluminum matrix due to the excellent plastic deformability and the work hardening during deformation. It should be noted that some dark areas were found on the fractograph, such as area I in Figures 7(a) and (d). According to the results of fracture location analysis, the interfacial fracture mainly occurs in sublayer II (points 1 through 4 in Table III). Nevertheless, sublayer I also consists of brittle intermetallic. In some local areas on the fractograph, fracture also occurred in sublayer I (points 5 through 8 in Table III).

#### E. Effects of the Parameters on Interfacial Thickness and Bonding Strength

The relationship between the thickness of the interface and its sublayers, interfacial shearing strength, and

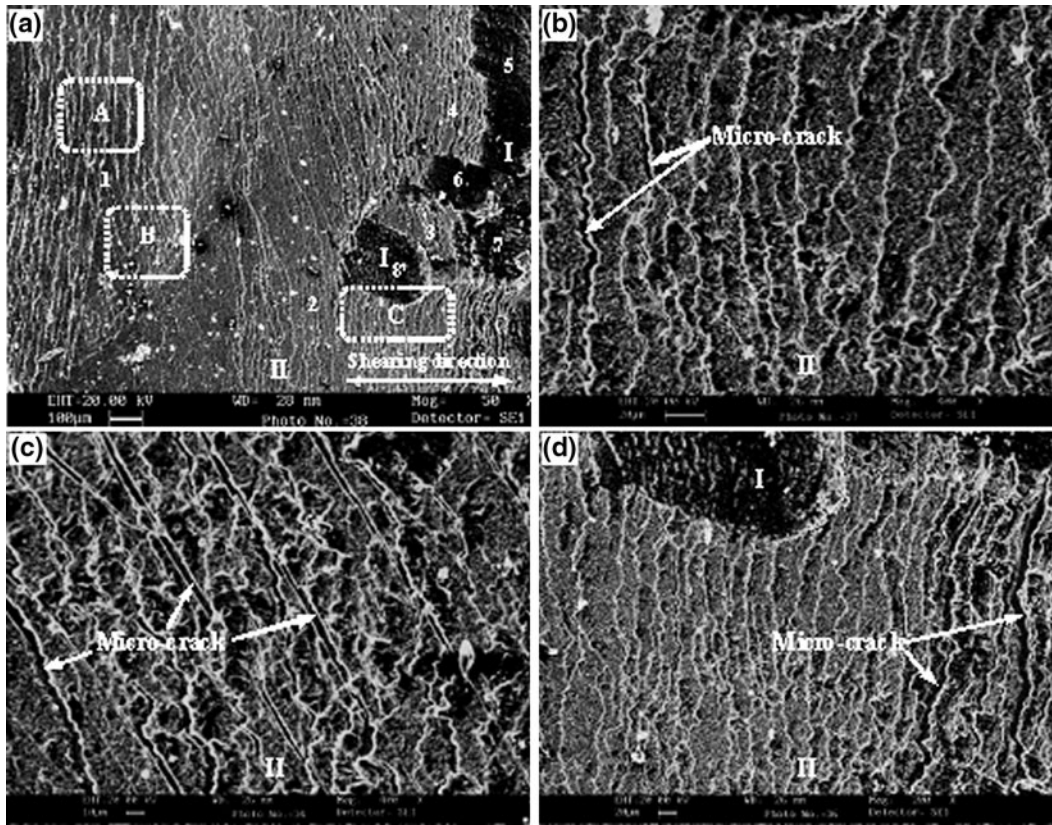


Fig. 7—SEM micrographs of the shear fractograph of the CCA rod (refer to Figs. 2 and 3): (a) shear fractograph of the deformed sample; and (b), (c), and (d) partial enlarged details of areas A, B, and C in (a), respectively.

Table III. Concentration of Cu and Al on Each Point on the Fracture (Reference to Fig. 7(a))

Point	1	2	3	4	5	6	7	8
$\omega_{Cu}$ , at. pct	30.37	32.62	32.17	30.37	62.73	60.12	57.66	55.27
$\omega_{Al}$ , at. pct	69.63	67.38	67.83	69.63	37.27	39.88	42.34	44.73
Location	sublayer II				sublayer I			

Note:  $\omega_{Cu}$  = the content of copper, and  $\omega_{Al}$  = the content of aluminum.

Table IV. Effects of the HCFC Processing Parameters on the Thickness and Bonding Strength of the Interface of CCA Rod

Main Processing parameter		$h_t$ ( $\mu\text{m}$ )	$h_I$ ( $\mu\text{m}$ )	$h_{II}$ ( $\mu\text{m}$ )	$h_{III}$ ( $\mu\text{m}$ )	$\tau$ (MPa)	Other Processing Parameters
$T_{Al}$ [K(°C)]	1043 (770)	160 ± 3	1.7 ± 0.1	2.8 ± 0.1	155.5 ± 2.6	45.2 ± 0.7	$Q_2 = 600$ L/h $v = 60$ mm/min
	1063 (790)	365 ± 2	1.6 ± 0.1	2.7 ± 0.1	360.7 ± 2.4	47.0 ± 0.5	
	1083 (810)	419 ± 3	1.4 ± 0.1	2.5 ± 0.1	415.1 ± 2.2	51.8 ± 0.4	
	1123 (850)	487 ± 3	1.3 ± 0.1	1.4 ± 0.1	484.3 ± 1.2	59.1 ± 0.6	
$Q_2$ (L/h)	600	402 ± 2	3.8 ± 0.1	29.9 ± 8.7	368.3 ± 3.9	40.5 ± 0.3	$T_{Al} = 1063$ K (790 °C) $v = 67$ mm/min
	700	276 ± 2	3.5 ± 0.1	17.5 ± 2.0	255.0 ± 4.1	43.4 ± 0.5	
	800	256 ± 2	1.8 ± 0.1	2.4 ± 0.1	251.8 ± 2.3	56.6 ± 0.3	
$v$ (mm/min)	67	276 ± 2	3.5 ± 0.1	17.5 ± 2.0	255.0 ± 4.1	43.4 ± 0.5	$T_{Al} = 1063$ K (790 °C) $Q_2 = 700$ L/h
	75	195 ± 3	1.7 ± 0.1	2.6 ± 0.1	190.7 ± 2.2	50.3 ± 0.2	
	87	75 ± 2	1.1 ± 0.1	0.1 ± 0.1	73.9 ± 0.2	67.9 ± 0.5	

$T_{Cu} = 1503$  K (1230 °C), and  $Q_1 = 600$  L/h.

HCFC processing parameters were summarized in Table IV. Under all the processing conditions in this work, all interfaces consisted of three sublayers, *i.e.*,

sublayers I, II, and III (Figure 4). Table IV shows that the total thickness of the interface ( $h_t$ ), the thicknesses of sublayers I( $h_I$ ), II( $h_{II}$ ), and III( $h_{III}$ ), and  $\tau$  were

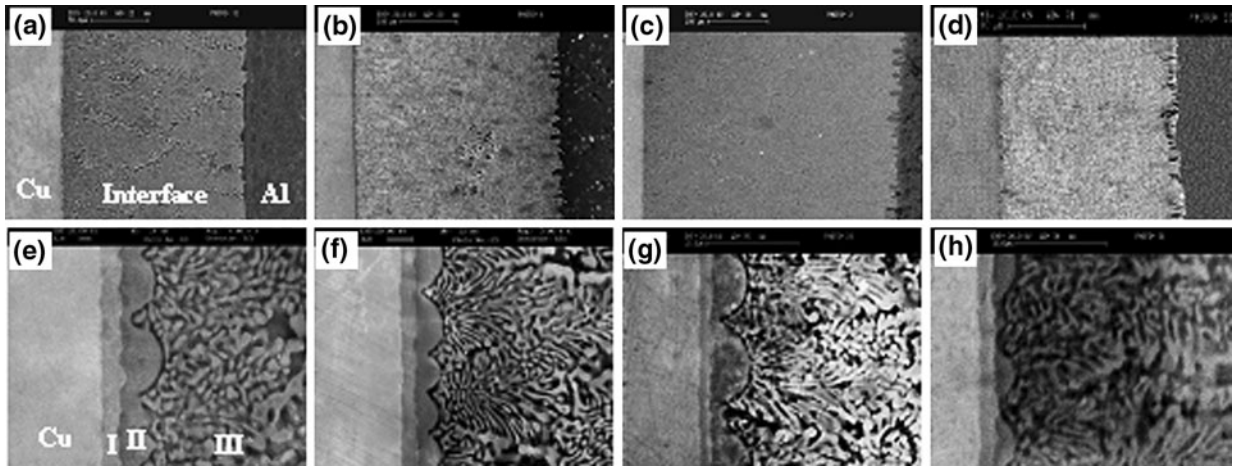


Fig. 8—SEM micrographs of the interface of CCA rods prepared at different aluminum casting temperatures: (a) and (e)  $T_{Al} = 1043$  K (770 °C), (b) and (f)  $T_{Al} = 1063$  K (790 °C), (c) and (g)  $T_{Al} = 1083$  K (810 °C), and (d) and (h)  $T_{Al} = 1123$  K (850 °C). (a) through (d) Correspond to experiments 1 through 4 in Table I, respectively. I—sublayer I, II—sublayer II, and III—sublayer III.

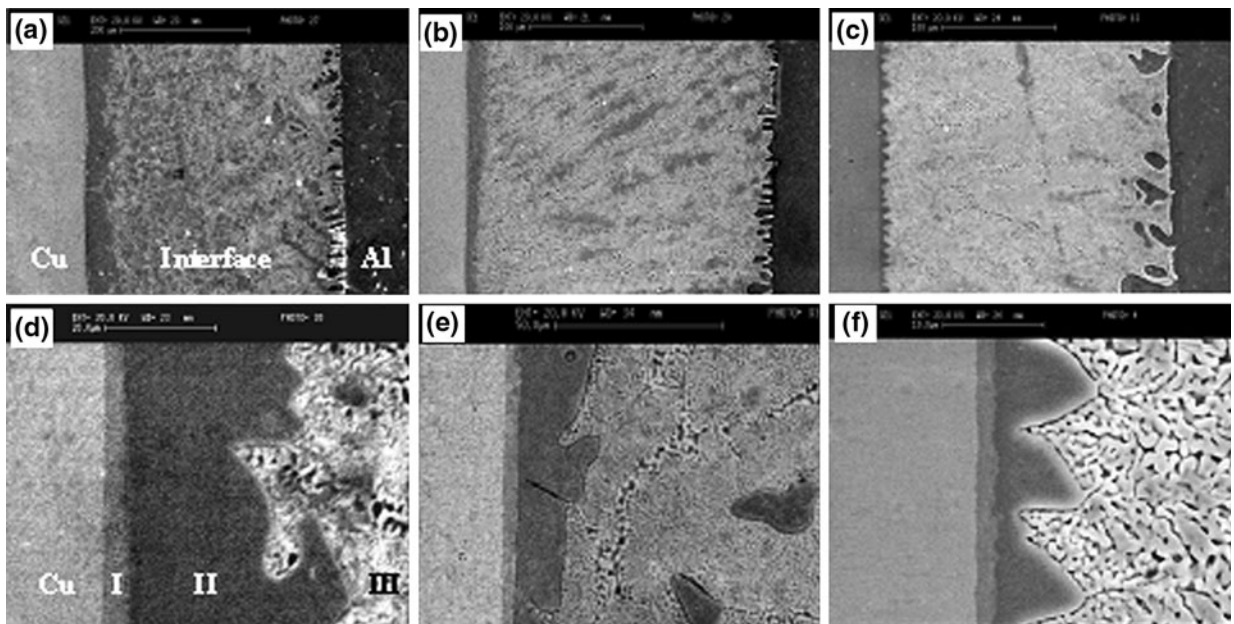


Fig. 9—SEM micrographs of the interface of CCA rods prepared under different secondary cooling water fluxes: (a) and (d)  $Q_2 = 600$ L/h, (b) and (e)  $Q_2 = 700$ L/h, and (c) and (f)  $Q_2 = 800$ L/h. (a) through (c) Correspond to experiments 5 through 7 in Table I, respectively. I—sublayer I, II—sublayer II, and III—sublayer III.

remarkably affected by aluminum casting temperature, secondary cooling intensity, and mean withdrawing speed.

#### 1. Effects of aluminum casting temperature

Figure 8 showed the microstructure of the interface of CCA rods prepared at different  $T_{Al}$ . Figures 8(a) through (d) correspond to experiments 1 through 4 in Table I, respectively. Figure 8 indicated that  $T_{Al}$  remarkably affected the morphology of sublayer II of the interface. When  $T_{Al} \leq 1083$  K (810 °C), sublayer II had continuous cellular-shape morphology with a semi-circle-like boundary with sublayer III (Figures 8(e) through (g)). However, when  $T_{Al} = 1123$  K (850 °C),

the microstructure of sublayer II was discontinuous and consisted of many scatter islands (Figure 8(h)).

From Table IV, one can find that  $h_{III}$ ,  $h_t$ , and  $\tau$  increased, while  $h_I$  and  $h_{II}$  decreased with the increase in  $T_{Al}$ . When  $T_{Al} = 1123$  K (850 °C),  $h_{III}$ ,  $h_t$ , and  $\tau$  reached the maximums, *i.e.*, 484.3  $\mu$ m, 487  $\mu$ m, and 59.1  $\pm$  0.6 MPa, while  $h_I$  and  $h_{II}$  reduced to the minimums, which were 1.3 and 1.4  $\mu$ m.

#### 2. Effects of the secondary cooling intensity

Figure 9 illustrated the microstructure of the interface of CCA rods prepared under different  $Q_2$ . Figures 9(a) through (c) correspond, respectively, to experiments 5



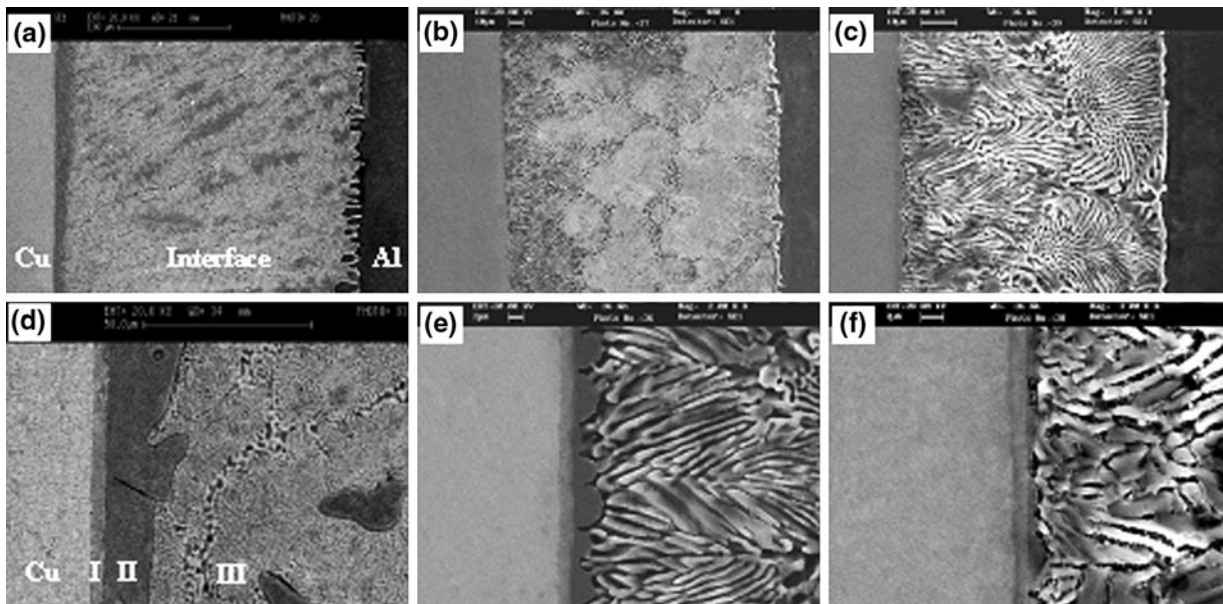


Fig. 10—SEM micrographs of the interface of CCA rods prepared at different mean withdrawing speeds: (a) and (d)  $v = 67$  mm/min, (b) and (e)  $v = 75$  mm/min, and (c) and (f)  $v = 87$  mm/min. (a) through (c) Correspond to experiments 6, 8, and 9 in Table I, respectively. I—sublayer I, II—sublayer II, and III—sublayer III.

through 7 in Table I. Figure 9 revealed that  $Q_2$  had a significant effect on the morphology of sublayer II. When  $Q_2 \leq 700$  L/h, sublayer II had a lamellar morphology (Figures 9(d) and (e)) with a irregular boundary with sublayer III (Figures 9(d) and (e)). However, when  $Q_2 = 800$  L/h, sublayer II illustrated a continuous cellular-like morphology (Figure 9(c)) with a zigzag boundary with sublayer III (Figure 9(f)).

Based on Table IV, with the rise of  $Q_2$ , the thicknesses of all sublayers decreased, but  $\tau$  increased. When  $Q_2 = 800$  L/h, the thickness of the three sublayers and  $h_t$  decreased to the minimums, *i.e.*,  $h_I = 1.8 \mu\text{m}$ ,  $h_{II} = 2.4 \mu\text{m}$ ,  $h_{III} = 251.8 \mu\text{m}$ , and  $h_t = 256 \mu\text{m}$ , while  $\tau$  achieved the maximum as  $56.6 \pm 0.3$  MPa.

### 3. Effects of the mean withdrawing speed

Figure 10 illustrated the microstructure of the interface of CCA rods prepared at different  $v$ . Figures 10(a), (b), and (c) correspond to experiments 6, 8, and 9 in Table I, respectively. Figure 10 suggests that the mean withdrawing speed exerted a remarkable influence on the microstructure of sublayer II. When  $v = 67$  mm/min, sublayer II had a lamellar morphology (Figure 10(a)) with an irregular boundary with sublayer III (Figure 10(d)). When  $v = 75$  mm/min, sublayer II formed a continuous cellular-shape structure (Figure 10(e)). However, when  $v = 87$  mm/min, sublayer II grew into a discontinuous islands-shape structure (Figure 10(f)).

According to Table IV, with the mean withdrawing speed increasing, the thickness of all sublayers decreased, but  $\tau$  increased. When  $v = 87$  mm/min, the thickness of the three sublayers and  $h_t$  reduced to the minimums, *i.e.*,  $h_I = 1.1 \mu\text{m}$ ,  $h_{II} = 0.1 \mu\text{m}$ ,  $h_{III} = 73.9 \mu\text{m}$ , and  $h_t = 75 \mu\text{m}$ , respectively, while  $\tau$  achieved the maximum,  $67.9 \pm 0.5$  MPa.

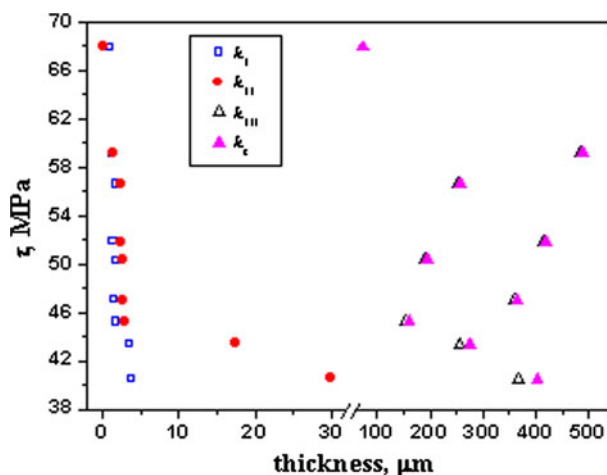


Fig. 11—Relationship between the total thickness of the interface and the thickness of each sublayer and the interfacial bonding strength,  $\tau$ .

Table IV revealed that, under the processing conditions in this work, the thickness of sublayer III, which occupied 92 to 99 pct of the total thickness of the interface, was much larger than that of sublayers I and II. The variations of both  $h_I$  and  $h_{II}$  had similar regulation with the changes of processing parameters, and those of  $h_{III}$  and  $h_t$  are the same against the processing parameters.  $Q_2$  and  $v$  had the same influence on the thicknesses of all sublayers, but  $T_{Al}$  has different effects on  $h_I$ ,  $h_{II}$  and  $h_{III}$ ,  $h_t$ .

According to the data tabulated in Table IV, the relationships between  $\tau$  and  $h_t$  and the thicknesses of every sublayer were plotted in Figure 11. Figure 11 showed that the variation of  $h_t$ - $\tau$  is similar to that of  $h_{III}$ - $\tau$ . That is,  $\tau$  varied irregularly with the change of  $h_t$  or  $h_{III}$ .

However,  $\tau$  declined rapidly with the rise of  $h_I$  and  $h_{II}$ . Therefore, the intermetallic compound layers ( $h_I$  and  $h_{II}$ ) controlled the interfacial bonding strength of CCA rod.

#### IV. DISCUSSION

The preceding experimental results and analyses indicated that the interface of CCA rod prepared by HCFC was formed by the interfacial reaction between the inner surface of copper sheath and liquid aluminum during the solidification of liquid aluminum core after filling in the presolidified copper sheath. The interface was composed of three sublayers—sublayer I was  $\text{Cu}_9\text{Al}_4$  layer, sublayer II was  $\text{CuAl}_2$  layer, and sublayer III was made up of  $\alpha\text{-Al}/\text{CuAl}_2$  pseudo eutectic (Figures 4 through 6). The dominative process of interfacial reaction was copper dissolving into liquid aluminum, because the reactants were liquid aluminum and solid copper. According to the Al-Cu binary alloy phase diagram,<sup>[15]</sup> when 2.48 at. pct  $< \omega_{\text{Cu}} < 31.97$  at. pct (5.65 wt pct  $< \omega_{\text{Cu}} < 52.5$  wt pct), Al-Cu binary alloy could form a pseudo eutectic phase consisting of  $\alpha\text{-Al}$  phase and  $\text{CuAl}_2$  phase at room temperature. As known from Figure 4 and Table IV, sublayer III was composed of  $\alpha\text{-Al}$  phase and  $\text{CuAl}_2$  phase and occupied more than 90 pct of the total thickness of the interface. Thus, one can believe that sublayer III was formed through copper dissolving from the inner surface of the sheath into liquid aluminum and then occurring in the eutectic reaction of liquid Al-Cu binary alloy during the continuous cooling process of CCA rod. Considering the forming mechanism of sublayer III is a combined action of the dissolution and diffusion of Cu and the convection and the diffusion coefficient of the metal atom in liquid metal is five to six orders larger than that in solid metal,<sup>[16]</sup> the interaction time and temperature of solid copper and liquid aluminum dominated  $h_{III}$  and  $h_t$ . In other words, the higher the interface temperature is or the longer the interaction time is, the more copper atoms dissolve into liquid aluminum and the larger  $h_{III}$  and  $h_t$  are. Therefore, either raising  $T_{Al}$  or decreasing  $Q_2$  or reducing  $v$  could cause the rise of  $h_{III}$  and  $h_t$  (Table IV).

Since sublayer II was thinner and appeared cellular-like or with lamellar morphology, which protruded from the boundary of sublayers I and II to sublayer III (Figure 4(b)), and there was no distinct concentration gradient and constant Cu/Al ratio within the sublayer (Figures 5(e) and (f)), one can think that sublayer II formed through the solidification and growth of  $\text{CuAl}_2$  phase from the inner surface of the sheath to sublayer III before sublayer III solidified. Therefore, the growth time of  $\text{CuAl}_2$  phase was determined by the cooling speed of CCA rod; *i.e.*, the higher the cooling speed is, the shorter the growth time of  $\text{CuAl}_2$  phase is and the less  $h_{II}$  is. Raising  $T_{Al}$  or  $v$  would make the solidification front of liquid aluminum move toward the exit of the composite mold, resulting in shortening the distance from the solidification front to the secondary cooling zone and increasing the cooling speed. Moreover, augmenting  $Q_2$  also increased the cooling speed.

Therefore,  $h_{II}$  remarkably reduced when  $T_{Al}$  or  $Q_2$  or  $v$  was raised (Table IV).

Sublayer I, which formed under all processing conditions in this work, was very thin ( $< 4 \mu\text{m}$ ) with straighter boundaries on both sides (Figure 4(b)), and there was a sharp radial concentration gradient of Cu (or Al) in it (Figures 5(e) and (f)). The concentration gradient in sublayer I and no concentration gradient in sublayers II and III implied that the formation mechanism of sublayer I is different from other sublayers. One can deem that Cu atoms diffused continuously into the  $\text{CuAl}_2$  layer (sublayer II) after the  $\text{CuAl}_2$  phase solidified and induced a solid-state phase transformation from  $\text{CuAl}_2$  phase to  $\text{Cu}_9\text{Al}_4$  phases; then sublayer I formed. Sublayer I formed through solid-state diffusion and phase transformation after the formation of sublayer II. The controlling factor of  $h_I$  was the cooling speed of CCA rod. Thus, the variation of  $h_I$  with HCFC processing parameters was similar to that of  $h_{II}$ .

Because the interface of CCA rod formed at higher temperature, copper atoms could dissolve into liquid aluminum with great diffusion speed. Consequently, the total thickness of the interface of CCA rods fabricated by HCFC reached more than  $75 \mu\text{m}$  (Table IV), which guaranteed a strong metallurgical bonding between the sheath and aluminum core. Because sublayer III formed by pseudo-eutectic reaction and  $\alpha\text{-Al} + \text{CuAl}_2$  phase can generate simultaneously in a wide range of 2.5 at. pct  $< \omega_{\text{Cu}} < 32.0$  at. pct (5.7 wt pct  $< \omega_{\text{Cu}} < 52.5$  wt pct),<sup>[15]</sup>  $h_{III}$  was the largest. The formation of sublayer II was attributed to the nucleation of the  $\text{CuAl}_2$  phase on the inner surface of the sheath and growth toward sublayer III before the solidification of sublayer III. In addition, the growing time of sublayer II was short for a rapid cooling speed of HCFC, so  $h_{II}$  (actually  $h_I$  and  $h_{II}$ ) was small. The formation mechanism of sublayer I was the solid-state phase transformation of  $\text{CuAl}_2$  phase induced by continuous diffusion of copper into sublayer II after sublayer II solidified. Since the diffusion coefficient of the metal atom in solid metal is five to six orders smaller than that in liquid metal,<sup>[16]</sup> and the diffusion time is very short under a rapid cooling speed of HCFC,  $h_I$  was the smallest (Figure 4 and Table IV).

To sum up, the forming process of the interface of CCA rod prepared by HCFC was as follows: in the course of CCA rod fabrication, when the presolidified copper sheath contacted with liquid aluminum at higher temperature, copper rapidly dissolved from the inner surface of the sheath into liquid aluminum and a zone of liquid Cu-Al binary alloy with a certain thickness and concentration gradient formed near the inner surface of the sheath. With the continuous withdrawal of CCA rod, the liquid Cu-Al alloy zone promptly moved into the forced cooling zone (the secondary cooling zone) and rapidly solidified into the interface. In the process of solidification, at first,  $\text{CuAl}_2$  phase nucleated on the inner surface of the sheath and grew toward the liquid aluminum core (Figure 12(a)). At the same time, the copper atom constantly diffused from the inner surface of the sheath to the liquid aluminum core *via* the solidified  $\text{CuAl}_2$  phase. When  $\omega_{\text{Cu}} > 69.2$  at. pct ( $\omega_{\text{Cu}} > 48.9$  wt pct),  $\text{CuAl}_2$  phase transformed into  $\text{Cu}_9\text{Al}_4$

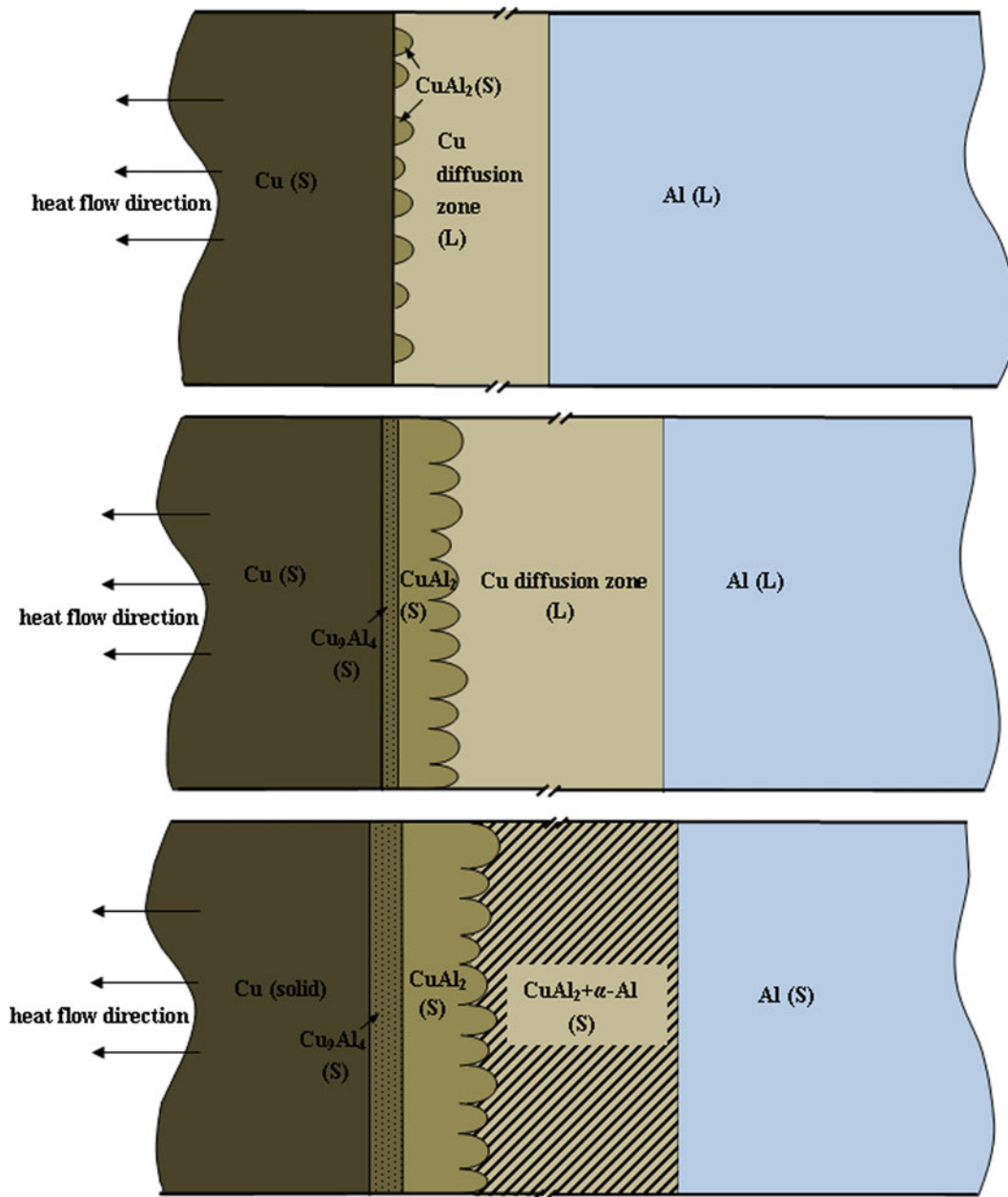


Fig. 12—Schematic diagram of the forming process of the interface of the CCA rod (S—solid, and L—liquid).

phase by solid-state phase transformation (Figure 12(b)). When the interfacial temperature fell below the eutectic temperature of liquid Cu-Al alloy [821.2 K (548.2 °C)],  $\alpha$ -Al + CuAl<sub>2</sub> pseudo eutectic was formed in the zone that had 2.5 at. pct <  $\omega_{Cu}$  < 32.0 at. pct (5.7 wt pct <  $\omega_{Cu}$  < 52.5 wt pct) (Figure 12(c)).

It has been reported that there is a close relationship between the interfacial bonding strength of Cu-Al composite and the phase composition and the thickness of each sublayer of the interface.<sup>[13]</sup> From the preceding results of this work, one can see that all the sublayers of the interface of CCA rod prepared by HCFC contained intermetallic compounds. The intermetallic compounds badly affect the interfacial mechanical properties of the composite owing to its high hardness and poor plasticity.

When the composite deformed, microcracks would readily form in intermetallic compounds and result in the failure of the composite. In general, the interfacial bonding strength decreases with the increase in the thickness of the intermetallic compound layer.<sup>[13]</sup> Although sublayer III is the thickest sublayer in the interface of the CCA rod, it contained a large amount of  $\alpha$ -Al phase besides CuAl<sub>2</sub> intermetallic compound, and  $\alpha$ -Al phase has a good plasticity and is interlaced with CuAl<sub>2</sub> phase (Figure 6(c)). This helps sublayer III to raise its resistance of plastic deformation. Since both sublayers I and II are composed of pure intermetallic compounds, the variation of the thicknesses would significantly affect the interfacial mechanical properties. It can be seen from Figure 11 that the interfacial

bonding strength sharply decreased at first and then decreased slowly with the rise of the thickness of the intermetallic compound sublayer (total thickness of sublayers I and II). This phenomenon is consistent with Abbasi's results.<sup>[13]</sup> Under HCFC processing conditions, in this work, a thinner intermetallic compound sublayer could be obtained. So the larger interfacial bonding strength could be achieved. While the thickness of the intermetallic compound sublayer (total thickness of sublayers I and II) is less than 4.3  $\mu\text{m}$ , the interfacial bonding strength is more than 50 MPa (Table IV and Figure 11). From the viewpoint of the interfacial bonding strength control, under a condition that equipment permitted, using a utmost mean withdrawing speed with a large enough cooling intensity would obtain CCA rods with the largest interfacial bonding strength, the thinnest intermetallic compound sublayer, and the thinnest interface. Furthermore, raising the mean withdrawing speed also helps to improve the productivity.

## V. CONCLUSIONS

In this work, the forming mechanism, the microstructure, and the bonding strength (shear strength) of the interface of CCA rods prepared by HCFC were studied, respectively, and the effects of main processing parameters, *e.g.*, aluminum casting temperature, the flux of the secondary cooling water and the mean withdrawing speed on the thickness, the microstructure, and the bonding strength of the interface, were analyzed in detail. Conclusions can be drawn as follows.

1. The interlayer of CCA rod was composed of three sublayers— $\text{Cu}_9\text{Al}_4$  layer (sublayer I),  $\text{CuAl}_2$  layer (sublayer II), and ( $\alpha\text{-Al}/\text{CuAl}_2$ ) pseudo eutectic layer (sublayer III). Sublayer I was formed by the mechanism of solid-state phase diffusion transformation. Both sublayer II and sublayer III were formed by the rapid solidification mechanism. The formation sequence of the three sublayers was sublayer II  $\rightarrow$  sublayer I  $\rightarrow$  sublayer III. The thickness of sublayer III, which occupied 92 to 99 pct of the total ones of the interlayer, is much larger than the thickness of sublayer I or II.
2. The interfacial bonding strengths of CCA rods were 40.5 to 67.9 MPa and met or exceeded the shear strength of pure aluminum. The thickness of the intermetallic compound sublayer (total thickness of sublayers I and II) was the major factor that controlled the interfacial bonding strength. The bonding strength fell with the rise of the thickness of the intermetallic compound sublayer.
3. The main processing parameters, *i.e.*, aluminum casting temperature, secondary cooling intensity, and mean withdrawing speed, have great influence on the microstructure and bonding strength of the

interface. Raising the aluminum casting temperature or the secondary cooling intensity or increasing the mean withdrawing speed resulted in a decrease in thickness of sublayers I and II with an increase in the interfacial bonding strength.

4. The optimum processing condition within the processing window of this work is as follows: copper casting temperature  $T_{\text{Cu}} = 1503 \text{ K}$  (1230  $^\circ\text{C}$ ), aluminum casting temperature  $T_{\text{Al}} = 1063 \text{ K}$  (790  $^\circ\text{C}$ ), primary cooling water flux  $Q_1 = 600 \text{ L/h}$ , secondary cooling water flux  $Q_2 = 700 \text{ L/h}$ , and mean withdrawing speed  $v = 87 \text{ mm/min}$ . Under the preceding processing conditions, the CCA rod with the thinnest interface thickness (75  $\mu\text{m}$ ) and the thinnest sublayer I and sublayer II (about 1.1 and 0.1  $\mu\text{m}$ ) has the largest interfacial bonding strength (67.9  $\pm$  0.5 MPa).

## ACKNOWLEDGMENTS

The authors are grateful for the financial support from the National High Technology Research and Development Program ("863" Program) of China (Grant No. 2009AA03Z532). The authors also thank Yong-Fu Wu, Yu Lei, Chao Wang, Jun Mei, and Bin Peng for their help with the experiments, Mrs. Run-Dong Xue for her help in SEM characterization, and Professor Zhi-Hao Zhang for many helpful discussions.

## REFERENCES

1. W. Perrard: *Wire J. Int.*, 2001, vol. 34, pp. 154–59.
2. K.Y. Rhee, W.Y. Han, H.J. Park, and S.S. Kim: *Mater. Sci. Eng. A*, 2004, vol. 384, pp. 70–76.
3. A. Gibson: *Wire J. Int.*, 2007, vol. 40, p. 73.
4. A. Gibson: *Wire J. Int.*, 2008, vol. 41, pp. 142–48.
5. N. Kazuyuki: *ISIJ Int.*, 1997, vol. 7, pp. 899–905.
6. M. Hiderita, T. Yamaguchi, and T. Takayama: U.S. Patent US03854193A, 1974-12-17.
7. N.F. Neumann: U.S. Patent 3421569, 1969.
8. J.X. Xie, C.J. Wu, C. Zhou, and Z.D. Wang: China Patent No. ZL01109076.6, 2003.
9. J.X. Xie, C.J. Wu, X.F. Liu, and X.H. Liu: *Mater. Sci. Forum*, 2007, vols. 539–543, pp. 956–61.
10. J.X. Xie, X.H. Liu, X.F. Liu, and Y.J. Su: China Patent ZL200610112817.3, 2008.
11. Y.J. Su, X.H. Liu, H.Y. Huang, C.J. Wu, X.F. Liu, and J.X. Xie: *Metall. Mater. Trans. B*, 2011, vol. 42B, pp. 104–13.
12. X.K. Peng, R. Wuhrer, G. Heness, and W.Y. Yeung: *J. Mater. Sci.*, 1999, vol. 34, pp. 2029–38.
13. M. Abbasi, T. Karimi, and M.T. Salehi: *J. Alloys Compd.*, 2001, vol. 319, pp. 233–41.
14. G. Heness, R. Wuhrer, and W.Y. Yeung: *Mater. Sci. Eng. A*, 2008, vols. 483–484, pp. 740–42.
15. Japan Institute of Metals: *Metals Data Book*, Maruzen Co., Ltd., Tokyo, 1993, p. 471.
16. D. Moreno, J. Garrett, and J.D. Embury: *Intermetallics*, 1999, vol. 7, pp. 1001–09.
17. Japan Institute of Metals: *Metals Data Book*, Maruzen Co., Ltd., Tokyo, 1993, p. 184.